



## Article

# Facts to Consider in Developing Materials That Emulate the Upper Jawbone: A Microarchitecture Study Showing Unique Characteristics at Four Different Sites

Ee Lian Lim <sup>1</sup>, Wei Cheong Ngeow <sup>1,\*</sup>, Kathreena Kadir <sup>1</sup> and Murali Naidu <sup>2</sup>

<sup>1</sup> Department of Oral and Maxillofacial Clinical Sciences, Faculty of Dentistry, University of Malaya, Kuala Lumpur 50603, Malaysia; elainelim@live.com.my (E.L.L.); kathreena@um.edu.my (K.K.)

<sup>2</sup> Department of Anatomy, Faculty of Medicine, University of Malaya, Kuala Lumpur 50603, Malaysia; murali\_naidu@um.edu.my

\* Correspondence: ngeowwy@um.edu.my; Tel.: +60-379674862

**Abstract:** The maxilla is generally acknowledged as being more trabecular than the mandible. Allograft currently available for use in the maxillofacial region is harvested from the hip and long bones, irrespective of their local characteristics, and grafted onto the jawbones. Other alternative are autograft or commercially available bone substitutes. Due to their inherent differences, an in-depth understanding of the bone microarchitecture is important to develop the most compatible graft for use at the maxilla. This cross-sectional study aimed to determine the microstructures of bone harvested from different sites of the maxilla, to be used for standard setting. Forty-nine specimens from seven human cadavers were harvested from the zygomatic buttress, anterior maxillary sinus wall, anterior nasal spine and anterior palate. Each bone block, measuring of 10 mm × 5 mm, was harvested using rotary instruments. Bone analysis was performed following micro-computed tomography to obtain trabecular number (Tb.N), trabecular separation (Tb.Sp), trabecular thickness (Tb.Th), and bone volume fraction (BV/TV). There were site-related differences, with BV/TV that ranged between 37.38% and 85.83%. The Tb.N was the lowest at the palate (1.12 (mm<sup>-1</sup>)) and highest at the anterior maxillary sinus wall (1.41 (mm<sup>-1</sup>)) region. The palate, however, had the highest trabecular separation value (Tb.Sp) at 0.47 mm. The Tb.Th was the lowest at the anterior nasal spine (0.34 mm) but both the zygoma and anterior maxillary sinus regions shared the highest Tb.Th (0.44 mm). Except for having the lowest Tb.Sp (0.35 mm), the anterior maxillary sinus wall consistently showed higher values together with the zygomatic buttress in all other parameters. Concurring with current clinical practice of harvesting autograft from the zygomatic buttress and anterior maxillary sinus wall, their bony characteristic serve as the microarchitecture standard to adopt when developing new bone graft materials for use in the maxilla.



**Citation:** Lim, E.L.; Ngeow, W.C.; Kadir, K.; Naidu, M. Facts to Consider in Developing Materials That Emulate the Upper Jawbone: A Microarchitecture Study Showing Unique Characteristics at Four Different Sites. *Biomimetics* **2023**, *8*, 115. <https://doi.org/10.3390/biomimetics8010115>

Academic Editors: Monica Dettin and Annj Zamuner

Received: 31 December 2022

Revised: 6 March 2023

Accepted: 8 March 2023

Published: 10 March 2023



**Copyright:** © 2023 by the authors. Licensee MDPI, Basel, Switzerland. This article is an open access article distributed under the terms and conditions of the Creative Commons Attribution (CC BY) license (<https://creativecommons.org/licenses/by/4.0/>).

**Keywords:** material; bone grafting; bone microarchitecture; maxilla; micro-computed tomography; trabecular bone

## 1. Introduction

Bone grafts are necessary to bridge bony maxillofacial defects caused by congenital deformity, pathology, trauma, and to restore bone resorption that occurs following tooth loss. Bone grafts and bone substitutes can be obtained from various sources using different techniques [1]. The gold standard is the transplantation of an autograft from another part of the patient's body. Alternatives includes an allograft that is sourced from genetically non-identical members of the same species, a xenograft that is sourced from genetically non-identical members of different species and alloplastic materials, i.e., synthetic bone substitutes that negate the use of human or animal products. To date, developing an ideal substitute for human bone in the oral and maxillofacial region remains the holy grail of bone graft research [2,3]. Recent advances in biomaterial technology, such as digital light

processing and partial infiltration, allows researchers to develop bioactive bone substitutes with the ability to control macroscopic pore size to 100–500  $\mu\text{m}$ , with strong interconnected porosity [4], but the product is far from being clinically proven.

An autologous bone graft remains the gold standard because of its osteogenic, osteoinductive, and osteoconductive properties. Besides proper surgical technique, its microarchitecture is a crucial parameter for the success of bone grafting. In general, intramembranous bone is preferred than endochondral bone as it is subjected to less resorption, thus improving retention and long-term stability, while inducing the body to produce natural bone [5]. A calvarium graft despite being intramembranous of origin, may need to be performed under sedation or general anaesthesia, which increases cost with higher morbidity [6]. Therefore, more complex surgical procedures involving extraoral sites are the least preferred method for bone grafting in implant or periodontal therapy in which the volume of bone needed may be small.

Intraoral donor sites are locations most dentists and dental specialists are familiar with. These sites are easily reachable, and harvesting can be accomplished under local anaesthesia in a standard dental office setting. There are usually no scars left behind and intraoral donor sites have lower morbidity than extraoral sites [7]. Autografts from mandibular symphysis and ramus are frequently used for intraoral bone reconstruction [8], but these sites are located on the mandible. Some studies describe the use of autografts from the maxilla, especially the tuberosity. Other sites of interest are the zygomatic buttress [9,10], the anterior maxillary sinus wall [11,12], the anterior nasal spine [13,14], and the anterior palate [15,16]. However, the maxilla is generally acknowledged as being more trabecular than the mandible, although it also has the benefit of being of intramembranous of origin. The microarchitecture properties at various sites of the maxilla remain poorly documented despite its significance to autograft regeneration [17]. This may hinder our efforts to develop compatible synthetic bone materials that mimics the maxillary bone.

The term “bone quality” has been widely used in the literature to describe different aspects of bone characteristics. The trabecular bone microarchitecture is an essential factor determining bone quality [18], in addition to chemical composition. In fact, one study correlated the type I–IV of bone with various parameters used to determine bone quality [19]. An in-depth understanding of bone microarchitecture is important to develop the most compatible graft for use at the maxilla, so as to enhance treatment outcome [20].

In the past, conventional histomorphometry was widely used to investigate the microarchitectural properties of bone. As well as being an invasive procedure, this technique is limited to two-dimensional results and is time-consuming. In addition, conventional histomorphometry is destructive in nature, as the samples are destroyed in the process, preventing the specimens being studied repetitively [18]. With the advancement of micro-computed tomography (micro-CT), the three-dimensional microstructure of the human bone can now be clearly visualized and studied. This non-destructive and high-resolution method can depict the trabecular network in various shades of grey colour based on the mineral content. Many studies have routinely applied micro-CT in the structural evaluations of trabecular microstructure [19,21–40].

The current study aimed to determine the bone quantity and quality at four sites of interest, namely the zygomatic buttress, anterior maxillary sinus wall, anterior nasal spine and anterior palate; the first two of which have been recommend as donor sites in clinical practice. The objective was to obtain their trabecular number (Tb.N), trabecular separation (Tb.Sp), trabecular thickness (Tb.Th), bone volume fraction (BV/TV), and their correlation with structure model index (SMI) using micro-CT for standard setting. Findings from this study will provide much-needed information on the optimum microarchitecture of bone when developing biomaterial for use in grafting the maxilla.

## 2. Materials and Methods

This cross-sectional study was conducted at the Department of Anatomy, Faculty of Medicine, University of Malaya, with the micro-CT study undertaken at the Nuclear

Agency Malaysia. The study received Institutional Board of Study approvals from the Faculty of Dentistry, University of Malaya [DF OS1814/0050(P)], and the Medical Research Ethics Committee, University of Malaya Medical Centre (MRECID.NO: 201865-6360). For the procurement of human bodies for the purpose of teaching and research in the university, consent was obtained based on the protocol adopted by the University of Malaya Medical Centre and approval by the Ministry of Health Malaysia. Seven human cadavers (all elderly males) previously embalmed and stored in 10% formalin solution (CH<sub>2</sub>O, 10%, Fisher Chemical) were obtained from the Department of Anatomy. Embalmed cadavers were stored between 6–12 months before use for research to ensure the tissues were fully fixed. The cadavers used in this study were thoroughly checked by the authors at the Department of Anatomy's Dissection Hall where the cadavers were kept, to ensure that the jaw bones were intact and free from any past trauma, malformation or pathology. The absence of lesion(s), sign of previous surgery, or reconstructive procedures at the areas of investigation was confirmed. The data collection period commenced in October 2018 and ended in April 2019. The authors studied all cadavers available at that time and did not calculate the sample size. This is a limitation of the current study.

We investigated bone microarchitecture at the zygomatic buttress, anterior maxillary sinus wall, anterior palate, and anterior nasal spine (ANS), as shown in Figure 1. Each bone block, with a dimension of 10 mm × 5 mm (but different thickness due to difference in site of origin), was harvested using a fine (0.5 mm) round bur mounted on a rotary hand piece with the speed of 1200 rpm. A total of 49 bone blocks were obtained, with 42 of them derived from the first three sites of interest, while only one bone block was retrieved from the ANS region of each cadaver.

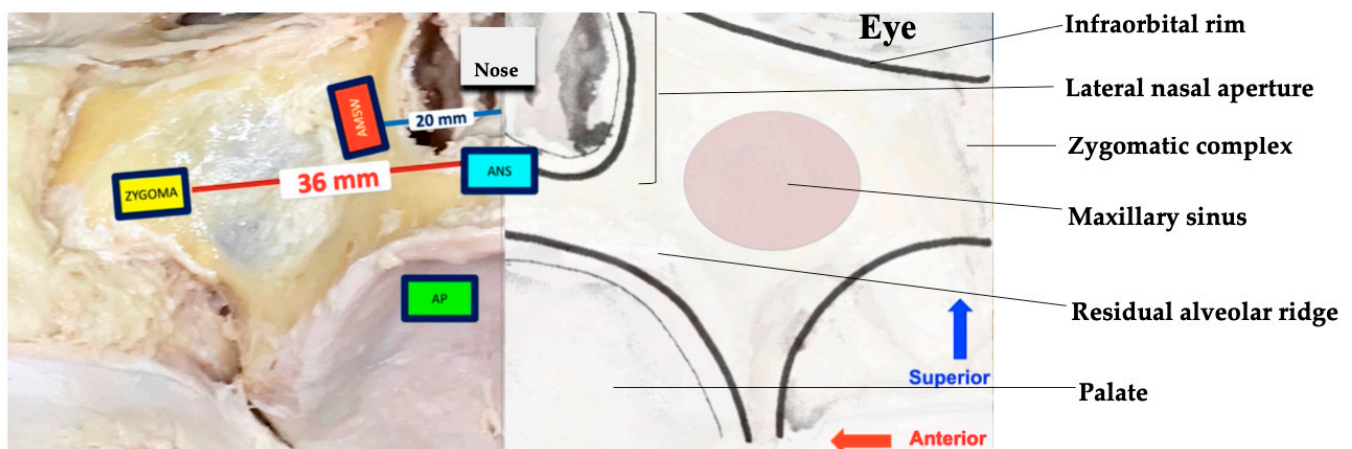


**Figure 1.** (Left) The four sites of interest in this study were the zygomatic buttress (ZYGOMA), anterior maxillary sinus wall (AMSW), anterior palate (AP), and anterior nasal spine (ANS). The location of the bone block was determined by using dental morphometrics. The average distance between the central incisor and the second premolar was approximately 36 mm, based on the mesiodistal sum teeth concerned. The average distance between central incisor and root apex of canine is approximately 20 mm. (Right) Anatomical scheme of the midface.

The sites of interest were identified using specific landmarks to ensure consistency. They were determined using the tooth size and dental arch dimension of southeast Asian Malay men as most of the cadavers were edentulous (Figure 1) [41]. The average distance from the central incisor to the second premolar was approximately 36 mm, hence the zygomatic buttress bone block was harvested at this distance bilaterally, 15 mm below the infraorbital rim. This location also corresponded with the hypothetical site of the bone graft harvesting site suggested by Lim et al., 2017 [42]. The average distance between central incisor and root apex of canines is approximately 20 mm, which is the reason the anterior maxillary sinus wall was identified as 20 mm from the midline. Bone blocks were harvested at 20 mm bilaterally. For the anterior palate, the bone blocks were harvested bilaterally at

2 mm from the bony crest, parallel to the tooth axis and 3 mm from the incisive foramen at the midline, following the description of Hassani et al. [43]. For the ANS region, only one bone block was harvested from each cadaver at 2 mm below its protrusion to avoid causing the collapse of the nose, based on descriptions from actual clinical practice.

The volume of the bone blocks harvested was measured using Archimedes' principle [44] as this water displacement technique ensures that the air and spaces within them are not included. These bone blocks were then dried, preserved, and were subjected to micro-CT scan (SkyScan 1172, Kontich, Belgium). Only 21 bone specimens were sent for micro-CT scan due to cost constraints. They were fixed in a cylindrical shaped styrofoam before being fitted and mounted onto a holder to minimize movements during scanning. The micro-CT scanning parameters were set at 35  $\mu\text{m}$  voxel size, 80 kVp, 124 mA, 0.5 mm aluminium filter, angular rotation step 0.70°, 180° scanning, with a total scan duration of 27 min and 43 s.

The micro-CT images were exported as TIFF files using NRecon (v 1.6, SkyScan, Kontich, Belgium) software for reconstruction and conversion into BMP images. Following this, they were imported into a trabecular bone analysis software, CTAn (v 1.15, SkyScan, Kontich, Belgium). The volume of interest (VOI) consisting of trabecular bone in each sample was delineated. The optimal threshold value for the images was determined using histogram analysis. Figure 2 shows a summary of the micro-CT bone analysis process.

Three-dimensional (3D) analysis was performed to acquire trabecular bone measurements, namely the bone volume fraction (BV/TV), trabecular number (Tb.N), trabecular thickness (Tb.Th), trabecular separation (Tb.Sp), and structure model index (SMI). The mean and standard deviation values were calculated using Microsoft Excel software (Version 2007, Microsoft, Redmond, WA, USA). The correlation of BV/TV, Tb.N, Tb.Th and Tb.Sp with structure model index (SMI) was determined. The trabecular bone parameters for the microarchitecture assessment are described in Table 1.

**Table 1.** Trabecular bone parameters for the microarchitecture assessment [45].

Abbreviation	Variable	Description	Standard Unit
TV	Total volume	Volume of the entire region of interest	$\text{mm}^3$
BV	Bone volume	Volume of the region segmented as bone	$\text{mm}^3$
BV/TV	Bone volume fraction	Ratio of the segmented bone volume to the total volume of the region of interest	%
Tb.N	Trabecular number	Measure of the average number of trabeculae per unit length	$\text{mm}^{-1}$
Tb.Th	Trabecular thickness	Mean thickness of trabeculae, assessed using direct 3D methods	mm
Tb.Sp	Trabecular separation	Mean distance between trabeculae, assessed using direct 3D methods	mm
SMI	Structure model index	An indicator of the structure of trabeculae	none

Statistical analyses were performed using SPSS Statistics 24.0 for Windows (SPSS, v.24.0, IBM, Chicago, IL, USA). Intra-observer reliability in measuring trabecular microstructure was performed using the intra-class correlation coefficient (ICC). Shapiro-Wilk test was done to verify the normality of data. Pearson's correlation coefficient was used to assess the relationship between the corresponding measurement parameters. The statistical differences in the volume of bone harvested from various regions and their measurement parameters were evaluated by analysis of variance (ANOVA) based on a 5% confidence level.

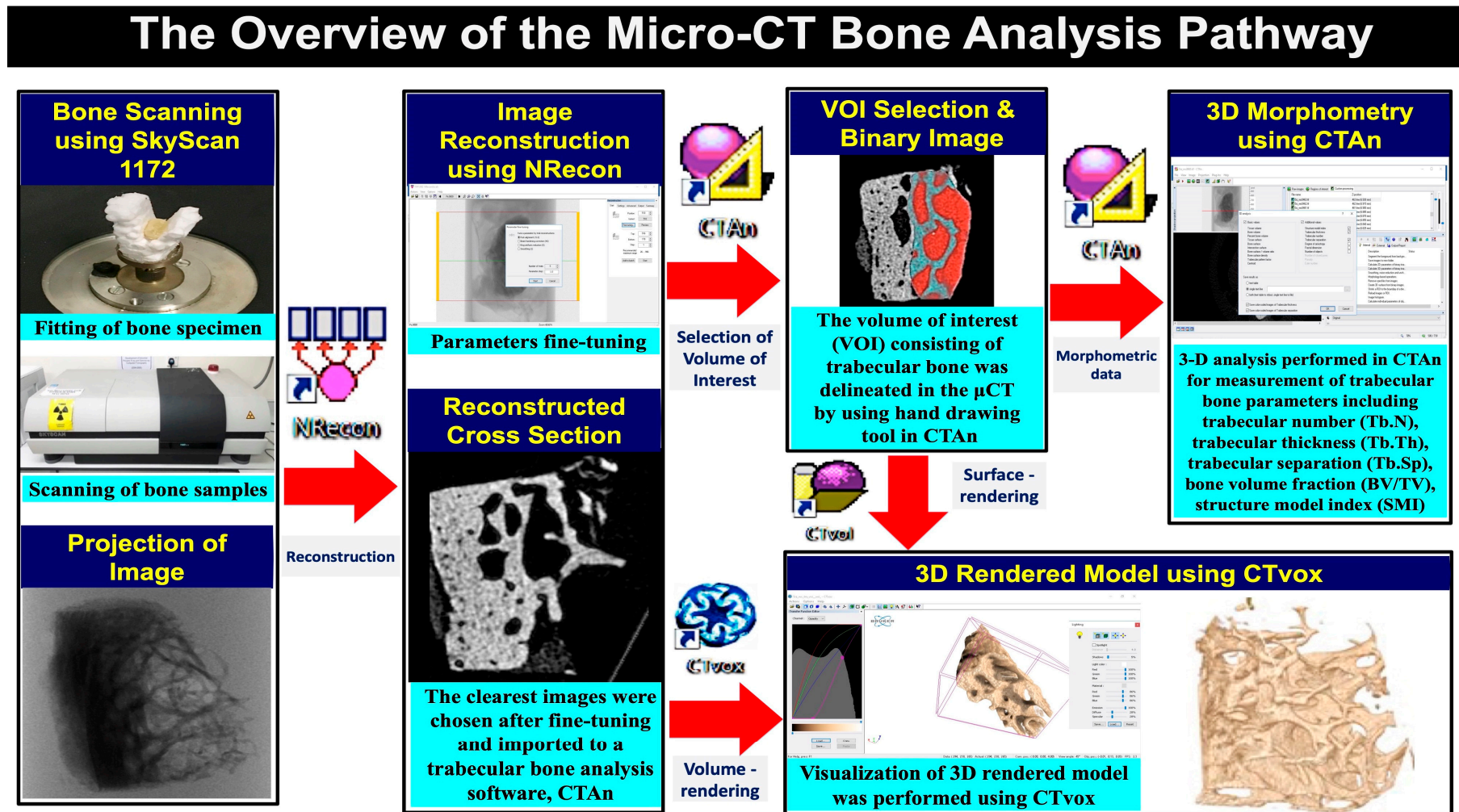


**Figure 2.** An overview of the micro-CT bone analysis process. All the steps were supported by SkyScan software. The steps for the micro-CT bone analysis pathway were bone scanning using SkyScan 1172, image reconstruction using NRecon, the volume of interest (VOI) selection and 3D morphometry acquisitions using CTAn. Visualization of the 3D rendered model was performed using CTvox or CTvol.

### 3. Results

The mean volume of bone harvested ranged from 0.10 mL to 0.25 mL. Surprisingly, there was no significant difference in the mean volume of bone harvested from the zygomatic buttress ( $0.15 \pm 0.05$  mL), anterior maxillary sinus wall ( $0.16 \pm 0.04$  mL), anterior palate ( $0.14 \pm 0.04$  mL) and anterior nasal spine region ( $0.14 \pm 0.05$  mL), despite their differences in thickness.

Figure 3 shows the reconstructed three-dimensional appearance of bone scanned using micro-CT. Table 2 shows the three-dimension (3-D) microarchitecture evaluation of the maxillary bone measured at these four different sites of interest. The intra-observer reliability showed a 0.999 intra-class correlation coefficient (ICC) (CI 0.998 to 0.999; Value 762.853, df 202;  $p < 0.001$ ), confirming good reliability of the measurements obtained. The average trabecular thickness (Tb.Th) was  $0.42 \pm 0.11$  mm, with a range of 0.24 to 0.57 mm. Both the zygomatic buttress and anterior maxillary sinus wall had the highest mean trabecular thickness at  $0.44 \pm 0.14$  mm and at  $0.44 \pm 0.09$  mm, respectively. ANS had the lowest mean trabecular thickness at  $0.34 \pm 0.11$  mm. Figure 4 presents the comparison of parameters between bone grafts taken from different donor sites.

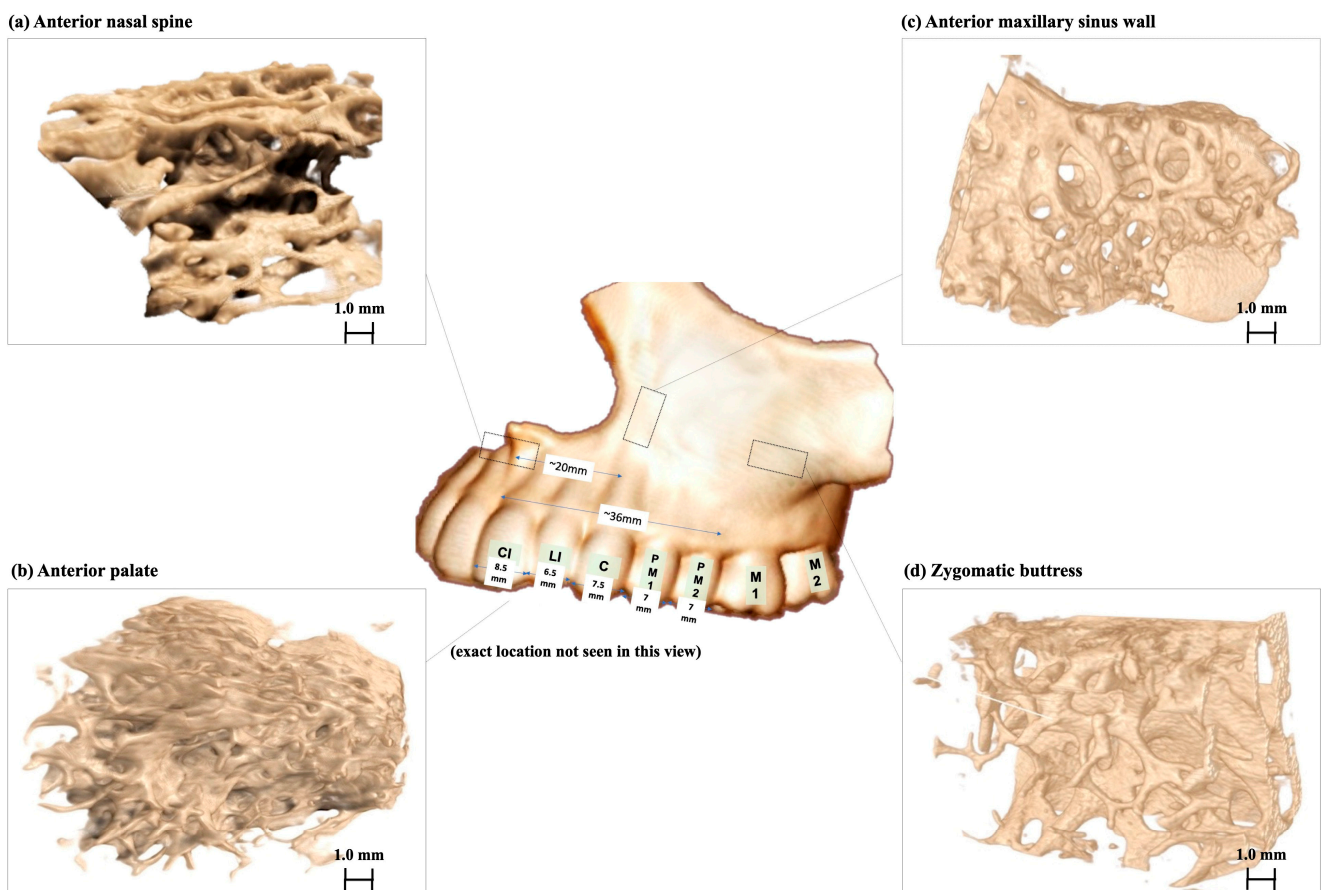


**Figure 3.** The reconstructed appearance of bone specimens visualised using CTvox software. (a) Anterior nasal spine, (b) anterior palate, (c) anterior maxillary sinus wall, (d) zygomatic buttress.

**Table 2.** Comparison of parameters between bone grafts taken from different donor sites (*n* = 21).

Donor Site	Mean ± SD	Minimum	Maximum	F	p-Value
Tissue Volume (mm <sup>3</sup> )				1.310	0.304
ZYGOMA	102.07 ± 52.83	27.21	199.57		
AMSW	76.31 ± 31.92	49.09	135.50		
AP	83.56 ± 26.79	51.09	113.23		
ANS	50.96 ± 24.63	27.21	76.38		
Overall	82.1 ± 38.32	27.21	199.57		
Bone Volume (mm <sup>3</sup> )				2.959	0.062
ZYGOMA	58.98 ± 29.17	23.25	93.17		
AMSW	44.31 ± 13.48	29.23	64.21		
AP	37.37 ± 12.09	23.27	51.47		
ANS	21.29 ± 8.08	15.03	30.40		
Overall	43.23 ± 21.41	15.03	93.17		
Bone Volume/Tissue Volume (%)				2.179	0.128
ZYGOMA	58.67 ± 21.16	38.59	85.83		
AMSW	60.11 ± 9.30	47.38	70.01		
AP	44.79 ± 4.43	38.38	52.08		
ANS	44.14 ± 9.68	37.38	55.23		
Overall	53.04 ± 14.31	37.38	85.83		
Structural Model Index				3.248	0.048 *
ZYGOMA	−2.51 ± 3.60	−7.11	0.46		
AMSW	−0.80 ± 0.83	−1.47	0.52		
AP	0.80 ± 0.31	0.46	1.27		
ANS	0.79 ± 0.14	0.63	0.87		
Overall	−0.63 ± 2.33	−7.11	1.27		
Trabecular Thickness (mm)				0.669	0.583
ZYGOMA	0.44 ± 0.14	0.25	0.57		
AMSW	0.44 ± 0.09	0.33	0.56		
AP	0.41 ± 0.09	0.27	0.53		
ANS	0.34 ± 0.11	0.24	0.45		
Overall	0.42 ± 0.11	0.24	0.57		
Trabecular Number (mm <sup>−1</sup> )				1.238	0.327
ZYGOMA	1.39 ± 0.36	0.71	1.74		
AMSW	1.41 ± 0.36	1.03	1.86		
AP	1.12 ± 0.21	0.86	1.40		
ANS	1.22 ± 0.03	1.19	1.23		
Overall	1.29 ± 0.30	0.71	1.86		
Trabecular Separation (mm)				0.692	0.570
ZYGOMA	0.44 ± 0.26	0.22	0.92		
AMSW	0.35 ± 0.10	0.23	0.50		
AP	0.47 ± 0.06	0.39	0.55		
ANS	0.41 ± 0.04	0.39	0.46		
Overall	0.42 ± 0.15	0.22	0.92		

\* Significant at *p*-value less than 0.05. F = Value of distribution, generated by dividing two mean squares to determine test significance. Note: the sites of interest in this study are the zygomatic buttress (ZYGOMA), anterior maxillary sinus wall (AMSW), anterior palate (AP), and anterior nasal spine (ANS).

One of the structure parameters, Tb.N, showed a value ranging from 0.71 to 1.86 mm<sup>−1</sup> for the different anatomical sites. The lowest mean value was observed at the anterior palate, at 1.12 ± 0.21 mm<sup>−1</sup> and the highest was at the anterior maxillary sinus wall (1.41 ± 0.36 mm<sup>−1</sup>). The anterior palate also had the lowest BV/TV (44.79 ± 4.43%), while the anterior maxillary sinus wall had the highest BV/TV (60.11 ± 9.30%). This contrasts with results observed for the Tb.Sp, which ranged from 0.22 to 0.92 mm. The anterior palate had the highest value of trabecular separation (0.47 ± 0.06 mm) while the anterior maxillary sinus wall had the lowest value (0.35 ± 0.10 mm). All together, these findings demonstrated that the anterior palate had the highest trabecular separation with the lowest trabecular number, and the lowest BV/TV.

All parameters showed no significant difference between different sites, except for structural model index (SMI) (F (3,17) = 3.248, *p* = 0.048), when analysed using one-way ANOVA. The post-hoc Dunnett T3 test revealed that the anterior maxillary sinus wall had a significantly lower SMI (−0.80 ± 0.83) compared to the anterior palate (0.80 ± 0.31). Similarly, ZYGOMA showed a significantly lower SMI (−2.51 ± 3.60) compared to the anterior palate (0.80 ± 0.31). In short, the anterior palate had the highest SMI.

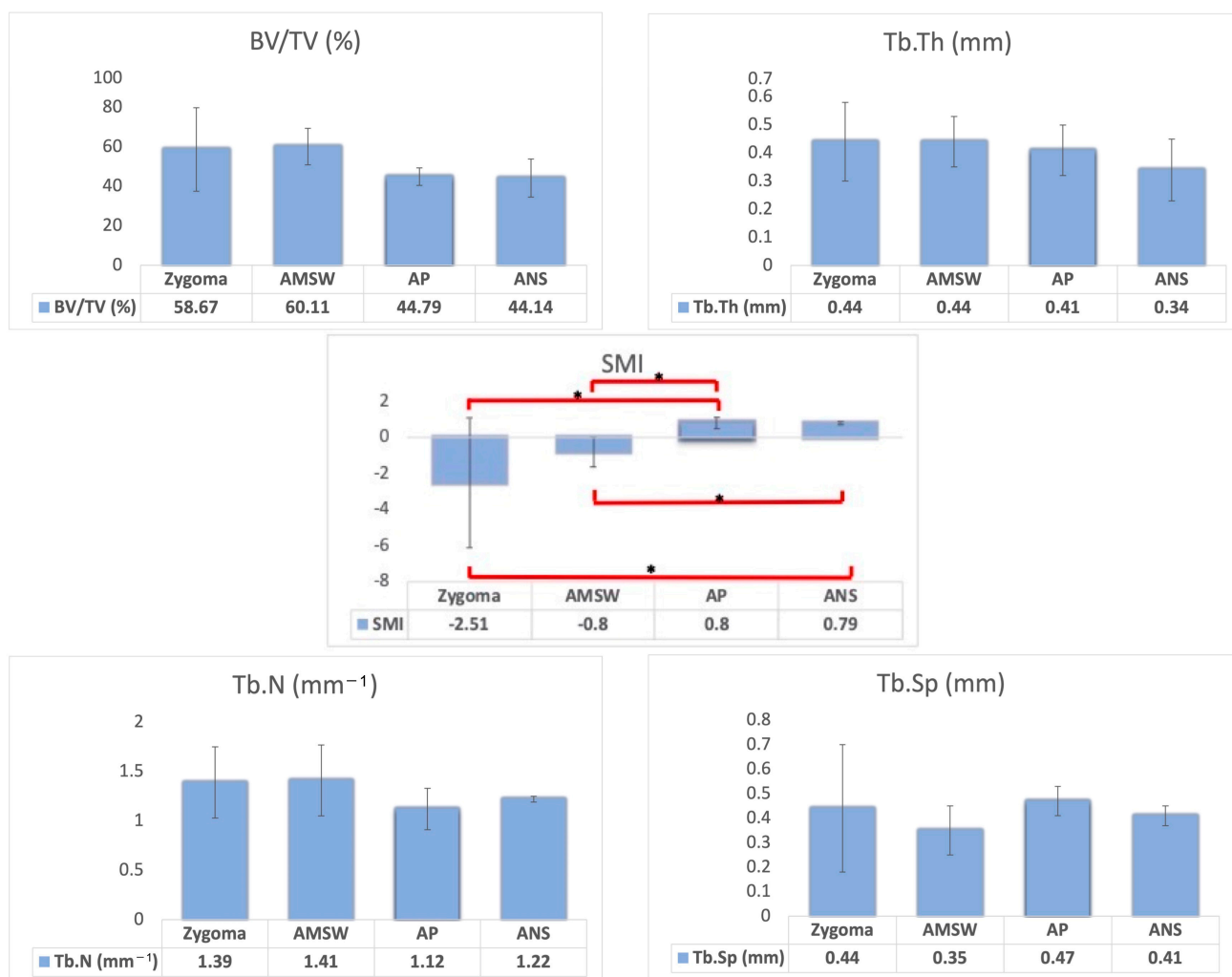


**Figure 4.** Comparison of parameters between bone grafts taken from different donor sites. \* ANOVA;  $p < 0.05$ . Note: The sites of interest in this study are the zygomatic buttress (ZYGOMA), anterior maxillary sinus wall (AMSW), anterior palate (AP), and anterior nasal spine (ANS).

Lastly, correlation analysis was done between different bone quality parameters [19,29,31]. BV/TV had a strong inverse correlation with trabecular separation (Tb.Sp) ( $r = -0.673$ ,  $p = 0.001$ ). The high negative correlation between BV/TV and Tsp. showed values of BV/TV higher than 50% squares with bones presenting most of their trabeculae separation less than 0.40 mm between each sample. BV/TV showed a moderate correlation with trabecular thickness (Tb.Th) ( $r = 0.547$ ,  $p = 0.01$ ). The positive correlation coefficient between BV/TV and Tb.Th shows a value of BV/TV higher than 50% squares, with bones presenting most of their trabeculae thicker than 0.40 mm.

SMI represents a measurement of surface convex curvature. There was a strong inverse correlation between SMI and BV/TV ( $r = -0.882$ ,  $p < 0.001$ ). In this study, 90.9% of bone specimens with BV/TV values lower than 50% showed a positive value of SMI, with a preponderance of values between 0 and 1 (plate-like trabeculae). Almost forty percent (38.10%) of bone specimens showed negative bone values, while 61.9% of bone specimens showed positive values. Only 4.76% of the bone had positive values between 1 and 2, with equal preponderance of plate-like and rod-like trabeculae.

SMI had a moderate inverse correlation with trabecular number (Tb.N) ( $r = -0.471$ ,  $p = 0.031$ ) and trabecular thickness (Tb.Th) ( $r = -0.414$ ,  $p = 0.062$ ). A poor direct correlation was recorded between trabecular separation (Tb.Sp) and trabecular thickness (Tb.Th) ( $r = 0.126$ ,  $p = 0.587$ ). Correlation studies help to identify the absence or presence of a

relationship between the trabecular bone parameters, but our findings suggest that there is no straightforward relationship within the parameters used in the analysis. This is possibly undermined by the unique characteristics at the four different sites as described above.

In summary, the microarchitecture demonstrated a high value of bone volume fraction, indicating good bone quality from the four sites of interest. Moreover, the high value of trabecular number and the normal mean value of trabecular separation indicated good compact structure at all four sites.

#### 4. Discussion

This study was performed on embalmed cadavers because of the difficulty in obtaining fresh human cadavers. Due to our tropical climate, which is hot and humid, fresh cadavers can undergo deterioration rapidly. Therefore, the cadavers were formalin-fixed as soon as possible after death [46]. Holm and Iazzo [47] highlighted that formalin fixation is still the most widely used and cost-effective technique for embalming human cadavers for education and medical research. Although there is evidence that formalin significantly alters the mechanical/biomechanical behaviour of ligaments, spine, and bone of animals, the histologic structure, density, and the mineral and lipid parameters do not seem to be affected [48]. Thus, this preservation method serves the purpose of the current study.

One of the limitations of this study was the lack of individual information on the donors' age and medical history. Thus, it was impossible to determine if the microarchitecture of bone blocks studied were affected by age or medical disorders that could alter bone quantity and quality.

Table 3 summarizes the microarchitecture at various human bone sites. Several studies have reported that the BV/TV ratio was the most significant parameter in determining bone quality [32]. Increased BV/TV was found in areas where great masticatory forces were received, as a result of optimal bone adaptation to the masticatory forces [32]. A greater value of BV/TV indicates a more compact structure that is able to resist the external forces transferred via mastication. The bone volume fraction (BV/TV) of the maxilla ranged from 13.53% to 48.70%, while that in the mandible ranged from 9.24 to 43.74%, depending on the site of study (see Table 3). The mean value of the BV/TV ( $53.04 \pm 14.31\%$  (range: 37.38–85.53%)) found in the present study was higher than other similar studies. Kim and Henkin [30], for example, reported the BV/TV values were  $14.59 \pm 7.68\%$  for maxilla and  $27.28 \pm 10.19\%$  for mandible with these values ranging from 6.75% to 48.92%. Parsa et al. attributed this difference to the difference in samples, ROI selections and the scanner system used [32].

The trabecular bone number (Tb.N), a parameter derived from the endosteal space architecture, is a good indicator of bone quality. In general, a high trabecular number suggests a more compact structure. The Tb.N of maxillary bone has been reported to be between 0.62 to 2.19  $\text{mm}^{-1}$ , while values in the mandible range between 0.007 and 2.19  $\text{mm}^{-1}$  (see Table 3). The present study reported a higher mean value that, nevertheless, falls within the range reported in the literature. However, the range of trabecular number reported in the literature is inconsistent, and in general were found to be higher in the Caucasians. One study reported that the cadaveric maxillary posterior regions had greater trabecular number ( $1.83 \pm 0.25 \text{ mm}^{-1}$ ) [36], while Kim and Henkin [30] reported greater values from the maxilla ( $2.07 \pm 0.80 \text{ mm}^{-1}$ ) and mandible ( $3.76 \pm 1.99 \text{ mm}^{-1}$ ). These differences could be attributed to bigger and denser bones among the Caucasians compared to the Asian population.

**Table 3.** Summary of the bony microarchitecture of various sites.

Authors (Year)	Population	Mean Age (Range)	n */N **	Method	Site(s)	Variable (If Any)	BV/TV (%)	Tb.N (1/mm)	Tb.Th (mm)	Tb.Sp (mm)
Muller et al., 1998 [21]	American	68 ± 16 (23–92)	70	micro-CT	Transiliac bone		14.48 ± 5.34	-	0.11 ± 0.02	0.77 ± 0.35
Giesen & Van Eijden, 2000 [22]	Dutch	72.6 ± 11.2 (56–89)	99 (11)	micro-CT	Condyles		17.00 ± 5.00	1.66 ± 0.26	0.10 ± 0.02	0.52 ± 0.13
Moon et al., 2004 [23]	Korean	55.1 (29–75)	10	micro-CT	Mandible (Alveolar Bone)		43.74 ± 16.04	1.27 ± 0.24	0.31 ± 0.08	0.51 ± 0.14
					Mandible (Basal Bone superior to mandibular canal)		20.39 ± 6.45	0.90 ± 0.23	0.28 ± 0.09	0.88 ± 0.20
					Mandible (Basal Bone inferior to mandibular canal)		9.24 ± 7.11	0.70 ± 0.20	0.22 ± 0.05	1.31 ± 0.42
Kato et al., 2005 [24]	Japanese	79.6	56 (28)	micro-CT	Jugale		23.2 ± 4.3	0.16 ± 0.05	1.53 ± 0.48	0.56 ± 0.20
					Middle point		19.9 ± 5.4	0.15 ± 0.05	1.38 ± 0.33	0.62 ± 0.28
					Zygomaxillae		20.5 ± 6.5	0.15 ± 0.06	1.49 ± 0.40	0.58 ± 0.20
Siddiqi et al., 2013 [25]	New Zealander	80 (65–94)	16	micro-CT	Median Palate	Palate	42.9 ± 13.8	1.1 ± 0.3	0.4 ± 0.2	7.5 ± 4.7
Ulm et al., 2009 [26]	Austrian	77.58 ± 10.09	278 (128)	micro-CT	Maxillary Premolar	Premolar	38.1 ± 12.5	1.0 ± 0.6	0.5 ± 0.3	8.1 ± 5.6
					Mandible (lateral incisor)	Female	30.70 ± 9.91	1.50 ± 0.34	0.19 ± 0.05	0.46 ± 0.14
						Male	36.90 ± 12.40	1.77 ± 0.39	0.21 ± 0.06	0.38 ± 0.14
					Mandible (first premolar)	Female	24.50 ± 8.45	1.47 ± 0.43	0.17 ± 0.04	0.57 ± 0.20
						Male	35.90 ± 13.62	1.58 ± 0.32	0.22 ± 0.06	0.82 ± 0.27
					Mandible (first molar)	Female	20.90 ± 9.65	1.22 ± 0.37	0.17 ± 0.04	0.72 ± 0.28
						Male	24.50 ± 7.93	1.38 ± 0.30	0.17 ± 0.04	0.58 ± 0.18
Blok et al., 2012 [27]	Dutch	73.7 ± 12.5	10	micro-CT	Maxilla		24.0 ± 13.0	1.57 ± 0.56	0.20 ± 0.05	0.69 ± 0.24
Kim et al., 2013 [28]	Korean	NA	69 (4)	micro-CT	Mandible		37.0 ± 18.0	1.50 ± 0.42	0.29 ± 0.11	0.71 ± 0.25
					Anterior Maxilla		21.35 ± 5.18	0.99 ± 0.23	0.22 ± 0.05	0.72 ± 0.16
					Posterior Maxilla		17.68 ± 6.21	0.89 ± 0.27	0.20 ± 0.07	0.79 ± 0.14
					Anterior Mandible		23.87 ± 7.68	0.72 ± 0.312	0.33 ± 0.05	0.85 ± 0.13
					Posterior Mandible		18.46 ± 9.44	0.78 ± 0.26	0.23 ± 0.07	0.82 ± 0.27
González-García & Monje, 2013 [29]	Spanish	51.56 ± 13.78 (20–79)	52 (31)	micro-CT	Maxilla		48.70 ± 17.85	2.19 ± 0.71	0.22 ± 0.06	0.31 ± 0.10
Kim & Henkin, 2015 [30]	American	NA	34 (12)	micro-CT	Maxilla		14.59 ± 7.68	2.07 ± 0.80	0.10 ± 0.02	0.63 ± 0.18
Bertl et al., 2015 [31]	Austrian	NA	36 (12)	micro-CT	Mandible		27.28 ± 10.19	3.76 ± 1.99	0.09 ± 0.02	0.42 ± 0.18
					Anterior Maxilla		27.15 ± 7.90	1.051 ± 0.20	0.26 ± 0.04	0.59 ± 0.13
					Posterior Maxilla		13.54 ± 3.40	0.624 ± 0.14	0.22 ± 0.03	0.89 ± 0.14
Parsa et al., 2015 [32]	Dutch	NA	20	micro-CT CBCT	Zygoma		26.79 ± 7.40	1.024 ± 0.20	0.26 ± 0.04	0.63 ± 0.13
					Mandible	micro-CT CBCT	32.35 ± 18.81 36.79 ± 23.17	- -	- -	- -
Kim et al., 2015 [33]	Korean	NA	68 (4)	micro-CT	Maxilla	Imaging Protocol				
					Mandible	19.37 μm 96.87 μm	18.53 ± 8.17 18.15 ± 8.60	0.24 ± 0.07 0.38 ± 0.11	0.77 ± 0.27 0.47 ± 0.17	0.83 ± 0.17 0.95 ± 0.19

Table 3. Cont.

Authors (Year)	Population	Mean Age (Range)	n */N **	Method	Site(s)	Variable (If Any)	BV/TV (%)	Tb.N (1/mm)	Tb.Th (mm)	Tb.Sp (mm)
Lee et al., 2017 [19]	Korean	75.7 (67–96)	116 (30)	micro-CT	Maxilla	Bone Density				
					Mandible	D1	37.29 ± 17.96	1.21 ± 0.45	0.30 ± 0.08	0.59 ± 0.22
Suttapreyasri et al., 2018 [35]	Thailand	>20	62 (41)	micro-CT CBCT	Maxilla	D2	27.46 ± 9.58	0.99 ± 0.24	0.28 ± 0.06	0.68 ± 0.14
					Mandible	D3	18.40 ± 10.20	0.71 ± 0.26	0.25 ± 0.05	0.82 ± 0.19
						D4	9.83 ± 8.02	0.41 ± 0.27	0.22 ± 0.06	1.20 ± 0.48
					Location	Anterior Maxilla	35.23 ± 10.68	-	-	-
						Posterior Maxilla	36.11 ± 9.15	-	-	-
						Anterior Mandible	63.25 ± 19.85	-	-	-
Posterior Mandible	46.74 ± 13.14	-	-	-						
Kulah et al., 2019 [36] Kivovics et al., 2020 [49]	Turkish	NA	17	micro-CT	Maxilla		32.65 ± 7.46	1.83 ± 0.05	0.28 ± 0.05	0.57 ± 0.13
	Hungarian	54.7 ± 6.5	16 (9)	micro-CT CBCT	Maxilla * Augmented sinus (grafted with allograft)	micro-CT CBCT	12.25 81.29	- -	0.15 1.82	0.88 0.85
Ibrahim et al., 2021 [37]	Dutch	NA	25	micro-CT	Mandible	micro-CT				
						Anterior	0.008 ± 0.003	0.005 ± 0.008	0.007 ± 0.008	-
				CBCT	Posterior	0.007 ± 0.004	0.004 ± 0.001	0.009 ± 0.001	-	
					Anterior	0.006 ± 0.002	0.007 ± 0.002	0.009 ± 0.003	-	
					Posterior	0.005 ± 0.003	0.006 ± 0.002	0.010 ± 0.004	-	
Tabassum et al., 2022 [38]	Malaysian	26.6 ± 5.9 (22–43)	20	CBCT	Mandible	CBCT	44.40 ± 14.77	0.44 ± 0.15	1.25 ± 0.55	2.05 ± 0.75
						Micro CT (Std)	46.01 ± 8.48	2.05 ± 0.46	0.24 ± 0.06	0.53 ± 0.11
Tayman et al., 2022 [39]	Turkey	NA	12	micro-CT CBCT	Posterior mandible	Micro CT (Hi)	44.28 ± 8.47	2.04 ± 0.47	0.23 ± 0.06	0.51 ± 0.11
						CBCT (Std)	57.13 ± 11.10	1.43 ± 0.25	0.46 ± 0.09	0.48 ± 0.12
						CBCT (Hi)	54.45 ± 11.98	1.43 ± 0.29	0.44 ± 0.09	0.46 ± 0.12
							21.01 ± 4.72	-	1.25 ± 0.55	0.35 ± 0.03
El-Gizawy et al., 2023 [40] Current study	USA	21	4 (1)	micro-CT	Distal femoral condyle					
	Malaysian	Elderly	49 (7)	micro-CT	Maxilla	Location				
						Zygoma	58.67 ± 21.16	1.39 ± 0.36	0.44 ± 0.14	0.44 ± 0.26
						AMSW	60.11 ± 9.30	1.41 ± 0.36	0.44 ± 0.09	0.35 ± 0.10
						AP	44.79 ± 4.43	1.12 ± 0.21	0.41 ± 0.09	0.47 ± 0.06
						ANS	44.14 ± 9.68	1.22 ± 0.03	0.34 ± 0.11	0.41 ± 0.04
						Mean	53.04 ± 14.31	1.29 ± 0.30	0.42 ± 0.11	0.42 ± 0.15

\* n is the number of specimens. \*\* N is the number of cadavers. CBCT = cone-beam computed tomography. NA = data (age) not available. Note: The sites of interest in this study are the zygomatic buttress (ZYGOMA), anterior maxillary sinus wall (AMSW), anterior palate (AP), and the anterior nasal spine (ANS).

The trabecular thickness (Tb.Th) of the maxillary bone has been reported to be between 0.10 to 0.50 mm, while values in the mandible range between 0.004 and 0.31 mm (see Table 3). In comparison to natural bone, the Tb.Th has been reported to be significantly thinner in the areas augmented with an allograft [50]. Values reported in the current study lean towards the higher end of the range, and are higher than the figures reported for the mandible.

Trabecular separation (Tb.Sp) is another indicator of bone quality. The trabecular separation (Tb.Sp) of maxillary bone has been reported to be between 0.31 to 0.89 mm, while values in the mandible has a range between 0.007 and 1.31 mm (see Table 3). By comparison, the value of trabecular separation found in the present study was lower than the D1 bone reported by Lee et al. [19], but had similar values to those reported by Kim and Henkin [30] for the mandibular region ( $0.42 \pm 0.18$  mm). As the trabecular separation reported here leaned towards D1 bone values, it can be concluded that the trabeculae were in close proximity, forming a compact trabecular bone structure. It is interesting that other authors reported greater trabecular separation value in the maxilla region ( $0.63 \pm 0.18$  mm) [28] and maxillary posterior region ( $0.57 \pm 0.13$  mm) [36], suggestive of variability in human jaw bone quality. The Tb.Sp value found in the present study is within the range of the optimal pore size for bone ingrowth (150–600  $\mu\text{m}$ ) [51]. This pore size is associated with better osteoconductivity, another important factor that cannot be overlooked when developing new biomaterials.

The parameter of SMI was described by Hildebrand & Rüegsegger (1997) to determine the 3D morphology of trabecular bone [52]. SMI represents a measurement of surface convex curvature by dilation of the 3D voxel model, that is, artificially adding one voxel thickness to all binarised object surfaces [52]. SMI is derived as follows:

$$\text{SMI} = 6 \times \left( \frac{S' \times V}{S^2} \right)$$

where  $S$  is the object surface area before dilation and  $S'$  is the change in surface area caused dilation.  $V$  is the initial, undilated object volume.

This parameter is crucial in osteoporotic degradation of trabecular bone that is characterized by the presence of rod- and plate-like structures in various configurations [53]. An ideal plate, cylinder and sphere have SMI values of 0, 3 and 4 respectively. In contrast, cylindrical and spherical cavities have SMI of  $-3$  and  $-4$  respectively [54]. The concave surfaces of closed cavities demonstrate the negative convexity for the calculation of SMI. Hence, bony regions containing greater numbers of enclosed cavities (usually regions with  $\text{BV}/\text{TV} > 50\%$ ) may have negative SMI values. In the current study, the mean value of SMI is  $-0.62 \pm 2.33$ , with a range of  $-7.11$  to  $1.27$ . The negative value of SMI seen in the zygomatic buttress ( $-2.51 \pm 3.60$ ) and anterior maxillary sinus wall ( $-0.80 \pm 0.83$ ) can be explained by the fact that these bones are solid and have a compact structure with a percent volume ( $\text{BV}/\text{TV}$ ) above 50%. Negative convexity to the SMI parameter was found in 38.10% of bone specimens among our series, indicating their origin from a denser bone [29,54]. Only 4.76% of the bone had positive values between 1 and 2, with equal preponderance of plate-like and rod-like trabeculae.

Bone quality at both the donor and recipient sites dictates treatment outcome in human donor autograft procedures. However, bone quality is independent of bone mass, as observed in bone with pathological disorder [55]. Therefore, the alternative is to use allograft, xenograft or synthetic bone material [1]. However, allografts currently available for use in dentistry are harvested from the hip and long bones and are grafted onto the jawbones irrespective of their local characteristics. The micro-architecture of trabecular bone has been proven to be among the crucial elements of bone quality, as it determines the bone healing rate. However, emulating this in synthetic material remains problematic.

Apart from particulate autogenous bone, demineralised freeze-dried bone allografts, deproteinized bovine bone allografts, synthetic  $\beta$ -tricalcium phosphate ( $\beta$ -TCP), anhydrous dicalcium phosphate (monetite), synthetic biphasic calcium phosphate (BCP), magnesium-enriched bioceramic, coralline-derived biomaterials, and porous titanium granules have

been studied clinically, with their microarchitecture analysed using micro-CT [49] However, all these bone graft materials have been shown to differ from the normal microarchitecture of the recipient sites in the maxilla and mandible in various microarchitecture parameters.

Therefore, the three-dimensional evaluation of human cadaver maxillary bone microarchitecture in this study allows for better understanding of the qualitative differences between the trabecular parameters among different sites, allowing researchers to appreciate their unique characteristics that differ from the mandible [56]. Concurring the current clinical practice of harvesting autografts from the zygomatic buttress and anterior maxillary sinus wall, their bony characteristic serve as the microarchitecture standard to adopt when developing new bone graft materials for use in the maxilla.

## 5. Conclusions

The quantity and quality of bone harvested from the zygomatic buttress, anterior maxillary sinus wall, anterior palate and anterior nasal spine were determined by a water displacement technique and a micro-CT scan, respectively. There was no significant difference in all bone parameters, with the exception of the SMI. Each site has its unique combinations of parameters. The BV/TV ranged between 37.38% and 85.83%, with anterior maxillary sinus wall > zygoma > palate > anterior nasal spine. The high values of bone volume fraction indicated good bone quality at the four sites of interest. The high value of trabecular number and the normal mean value of trabecular separation indicated good compact structure at all four sites. Except for having the lowest Th.Sp (0.34 mm), the anterior maxillary sinus wall consistently showed higher values together with the zygomatic buttress in all other parameters. Concurring with the current clinical practice of harvesting autografts from the zygomatic buttress and anterior maxillary sinus wall, their bony characteristic serve as the microarchitecture standard to adopt when developing new bone graft materials for use in the maxilla.

**Author Contributions:** Conceptualization, W.C.N., K.K. and M.N.; methodology, E.L.L., W.C.N., K.K. and M.N.; software, E.L.L., W.C.N., K.K. and M.N.; validation, E.L.L., W.C.N., K.K. and M.N.; formal analysis E.L.L.; investigation, E.L.L.; resources, E.L.L., W.C.N., K.K. and M.N.; writing—original draft preparation, E.L.L., W.C.N., K.K. and M.N.; writing—review and editing, E.L.L., W.C.N., K.K. and M.N.; visualization, E.L.L., W.C.N., K.K. and M.N.; supervision, W.C.N., K.K. and M.N.; project administration, E.L.L., W.C.N., K.K. and M.N.; funding acquisition, E.L.L., W.C.N., K.K. and M.N. All authors have read and agreed to the published version of the manuscript.

**Funding:** This research was funded by the Dental Faculty Research Grant, University of Malaya (Project No.: GPF001E-2019) and supported by the University of Malaya Student Financial Aid 2019 Scheme (UM.TNC2/IPPP/81/10/1).

**Institutional Review Board Statement:** This study received Institutional Board of Study approvals from the Faculty of Dentistry, University of Malaya [DF OS1814/0050(P)], and the Medical Research Ethics Committee, University of Malaya Medical Centre (MRECID.NO: 201865-6360).

**Informed Consent Statement:** For the procurement of human bodies for the purpose of teaching and research in the university, consent was obtained based on the protocol adopted by the University of Malaya Medical Centre and approval by the Ministry of Health Malaysia.

**Data Availability Statement:** No new data were created or analyzed in this study. Data sharing is not applicable to this article.

**Acknowledgments:** The authors wish to acknowledge the staffs from Department of Anatomy, Faculty of Medicine, University of Malaya, especially the former Head of Department, Normadhah Binti M Kassim for her kind support. Our sincere appreciation goes to Assoc. Lau Seng Fong from University Putra Malaysia for her help in image processing and Philip Salmon from Bruker-microCT, Kontich for his invaluable input in image acquisition.

**Conflicts of Interest:** The authors declare no conflict of interest.

## References

1. Cheah, C.W.; Al-Namnam, N.M.; Lau, M.N.; Lim, G.S.; Raman, R.; Fairbairn, P.; Ngeow, W.C. Synthetic Material for Bone, Periodontal, and Dental Tissue Regeneration: Where Are We Now, and Where Are We Heading Next? *Materials* **2021**, *14*, 6123. [[CrossRef](#)]
2. Labrés, X.R.; Camps, À.R.; Salas, E.J.; Alburquerque, R.; Ortega, E.V.; López, J.L. Graft materials in oral surgery: Revision. *Biomim. Biomater. Tissue Eng.* **2014**, *19*, 150–154.
3. Misch, C.M. *Autogenous Bone is Still the Gold Standard of Graft Materials in 2022*; The American Academy of Implant Dentistry: Chicago, IL, USA, 2022; Volume 48, pp. 169–170.
4. Wu, Y.; Chen, R.; Chen, X.; Yang, Y.; Qiao, J.; Liu, Y. Development of Strong and Tough  $\beta$ -TCP/PCL Composite Scaffolds with Interconnected Porosity by Digital Light Processing and Partial Infiltration. *Materials* **2023**, *16*, 947. [[CrossRef](#)]
5. Zins, J.E.; Whitaker, L.A.; Enlow, D.H. Membranous versus endochondral bone: Implications for craniofacial reconstruction. *Plast. Reconstr. Surg.* **1983**, *72*, 785. [[CrossRef](#)]
6. Sándor, G.K.; Nish, I.A.; Carmichael, R.P. Comparison of conventional surgery with motorized trephine in bone harvest from the anterior iliac crest. *Oral Surg. Oral Med. Oral Pathol. Oral Radiol. Endodontology* **2003**, *95*, 150–155. [[CrossRef](#)]
7. Borstlap, W.A.; Heidbuchel, K.L.; Freihofer, H.P.M.; Kuijpers-Jagtman, A.M. Early secondary bone grafting of alveolar cleft defects: A comparison between chin and rib grafts. *J. Cranio-Maxillofac. Surg.* **1990**, *18*, 201–205. [[CrossRef](#)]
8. Misch, C.M. Comparison of intraoral donor sites for onlay grafting prior to implant placement. *Int. J. Oral Maxillofac. Implant.* **1997**, *12*, 767–776.
9. Bassil, J.; Abi Sleiman, A.; Mrad, S.; Noujeim, Z. The Zygomatic Buttress as an Efficient Intraoral Donor Site for Limited Maxillary Reconstructions: A Case Series and Brief Literature Review. *Case Rep. Dent.* **2021**, *2021*, 5539185. [[CrossRef](#)] [[PubMed](#)]
10. Abdeltawab, A.R.; Dahaba, M.; Belal, S. Volumetric and linear assessment of maxillary, mandibular and zygomatic bone as donor sites for alveolar ridge augmentation using CBCT: A cross sectional study. *Int. J. Health Sci.* **2022**, *6* (Suppl. S4), 1185–1193. [[CrossRef](#)]
11. Emodi, O.; Nseir, S.; Shilo, D.; Srouji, H.; Rachmiel, A. Antral Wall Approach for Reconstruction of Orbital Floor Fractures Using Anterior Maxillary Sinus Bone Grafts. *J. Craniofacial Surg.* **2018**, *29*, e421–e426. [[CrossRef](#)]
12. Hwang, J.W.; Han, M.S.; Kang, S.H.; Kwak, J.W.; Kim, H.K.; Kim, T.H.; Lee, S.H. Long-term outcomes of nasoseptal perforation repair using anterior maxillary sinus wall as an interpositional graft. *Am. J. Rhinol. Allergy* **2022**, *36*, 238–244. [[CrossRef](#)] [[PubMed](#)]
13. Cho, Y.S.; Hwang, K.G.; Park, C.J. Postoperative effects of anterior nasal spine bone harvesting on overall nasal shape. *Clin. Oral Implant. Res.* **2013**, *24*, 618–622. [[CrossRef](#)] [[PubMed](#)]
14. Mayordomo, R.B.; Martínez, R.G.; Alfaro, F.H. The anterior maxilla as a potential source of bone grafts: A morphometric cone beam computed tomography analysis of different anatomical areas. *Int. J. Oral Maxillofac. Surg.* **2016**, *45*, 1049–1056. [[CrossRef](#)]
15. Safi, Y.; Behzadi, S.; Shafizadeh, M.; Amid, R.; Kadkhodazadeh, M. CBCT Evaluation of the maxillary palatine process as a donor site for the regeneration of periodontal defects. *J. Adv. Periodontol. Implant. Dent.* **2022**, *14*, 20. [[CrossRef](#)]
16. Joshi, S.; Desai, S.; Mudda, J.; Patil, V.; Mustafa, M. Estimation of height and width of bone in anterior hard palate as a donor site for autogenous bone graft using IOPA by long cone paralleling technique. *Niger. J. Clin. Pract.* **2020**, *23*, 1487. [[PubMed](#)]
17. Misch, C.E.; Qu, Z.; Bidez, M.W. Mechanical properties of trabecular bone in the human mandible: Implications for dental implant treatment planning and surgical placement. *J. Oral Maxillofac. Surg.* **1999**, *57*, 700–706. [[CrossRef](#)]
18. Burghardt, A.J.; Link, T.M.; Majumdar, S. High-resolution computed tomography for clinical imaging of bone microarchitecture. *Clin. Orthop. Relat. Res.* **2011**, *469*, 2179–2193. [[CrossRef](#)]
19. Lee, J.H.; Kim, H.J.; Yun, J.H. Three-dimensional microstructure of human alveolar trabecular bone: A micro-computed tomography study. *J. Periodontal Implant. Sci.* **2017**, *47*, 20–29. [[CrossRef](#)]
20. Misch, C.E. *Contemporary Implant Dentistry*; Elsevier Health Sciences: New York, NY, USA, 2007.
21. Müller, R.; Van Campenhout, H.; Van Damme, B.; Van der Perre, G.; Dequeker, J.; Hildebrand, T.; Rügsegger, P. Morphometric analysis of human bone biopsies: A quantitative structural comparison of histological sections and micro-computed tomography. *Bone* **1998**, *23*, 59–66. [[CrossRef](#)]
22. Giesen, E.; Van Eijden, T. The three-dimensional cancellous bone architecture of the human mandibular condyle. *J. Dent. Res.* **2000**, *79*, 957–963. [[CrossRef](#)]
23. Moon, H.-S.; Won, Y.-Y.; Kim, K.-D.; Ruprecht, A.; Kim, H.-J.; Kook, H.-K.; Chung, M.-K. The three-dimensional microstructure of the trabecular bone in the mandible. *Surg. Radiol. Anat.* **2004**, *26*, 466–473. [[CrossRef](#)] [[PubMed](#)]
24. Kato, Y.; Kizu, Y.; Tonogi, M.; Ide, Y.; Yamane, G.-Y. Internal structure of zygomatic bone related to zygomatic fixture. *J. Oral Maxillofac. Surg.* **2005**, *63*, 1325–1329. [[CrossRef](#)]
25. Siddiqi, A.; Kieser, J.A.; De Silva, R.K.; McNaughton, A.; Zafar, S.; Duncan, W.J. Trabecular bone microarchitecture in the median palate and maxillary premolar alveolar sites of edentulous elderly cadavers. *J. Oral Maxillofac. Surg.* **2013**, *71*, 1852.e1–1852.e11. [[CrossRef](#)] [[PubMed](#)]
26. Ulm, C.; Tepper, G.; Blahout, R.; Rausch-Fan, X.; Hienz, S.; Matejka, M. Characteristic features of trabecular bone in edentulous mandibles. *Clin. Oral Implant. Res.* **2009**, *20*, 594–600. [[CrossRef](#)] [[PubMed](#)]
27. Blok, Y.; Gravesteyn, F.; Van Ruijven, L.; Koolstra, J. Micro-architecture and mineralization of the human alveolar bone obtained with microCT. *Arch. Oral Biol.* **2013**, *58*, 621–627. [[CrossRef](#)]

28. Kim, J.E.; Shin, J.M.; Oh, S.O.; Yi, W.J.; Heo, M.S.; Lee, S.S.; Choi, S.C.; Huh, K.H. The three-dimensional microstructure of trabecular bone: Analysis of site-specific variation in the human jaw bone. *Imaging Sci. Dent.* **2013**, *43*, 227–233. [[CrossRef](#)]
29. González-García, R.; Monje, F. Is micro-computed tomography reliable to determine the microstructure of the maxillary alveolar bone? *Clin. Oral Implant. Res.* **2013**, *24*, 730–737. [[CrossRef](#)]
30. Kim, Y.J.; Henkin, J. Micro-computed tomography assessment of human alveolar bone: Bone density and three-dimensional micro-architecture. *Clin. Implant. Dent. Relat. Res.* **2015**, *17*, 307–313. [[CrossRef](#)]
31. Bertl, K.; Heimel, P.; Rökl-Riegler, M.; Hirtler, L.; Ulm, C.; Zechner, W. MicroCT-based evaluation of the trabecular bone quality of different implant anchorage sites for masticatory rehabilitation of the maxilla. *J. Cranio-Maxillofac. Surg.* **2015**, *43*, 961–968. [[CrossRef](#)]
32. Parsa, A.; Ibrahim, N.; Hassan, B.; van der Stelt, P.; Wismeijer, D. Bone quality evaluation at dental implant site using multislice CT, micro-CT, and cone beam CT. *Clin. Oral Implant. Res.* **2015**, *26*, e1–e7. [[CrossRef](#)]
33. Kim, J.-E.; Yi, W.-J.; Heo, M.-S.; Lee, S.-S.; Choi, S.-C.; Huh, K.-H. Three-dimensional evaluation of human jaw bone microarchitecture: Correlation between the microarchitectural parameters of cone beam computed tomography and micro-computer tomography. *Oral Surg. Oral Med. Oral Pathol. Oral Radiol.* **2015**, *120*, 762–770. [[CrossRef](#)]
34. Hsu, P.-Y.; Tsai, M.-T.; Wang, S.-P.; Chen, Y.-J.; Wu, J.; Hsu, J.-T. Cortical bone morphological and trabecular bone microarchitectural changes in the mandible and femoral neck of ovariectomized rats. *PLoS ONE* **2016**, *11*, e0154367. [[CrossRef](#)]
35. Suttapreyasri, S.; Suapear, P.; Leepong, N. The accuracy of cone-beam computed tomography for evaluating bone density and cortical bone thickness at the implant site: Micro-computed tomography and histologic analysis. *J. Craniofacial Surg.* **2018**, *29*, 2026–2031. [[CrossRef](#)]
36. Kulah, K.; Gulsahi, A.; Kamburoğlu, K.; Geneci, F.; Ocak, M.; Celik, H.H.; Ozen, T. Evaluation of maxillary trabecular microstructure as an indicator of implant stability by using 2 cone beam computed tomography systems and micro-computed tomography. *Oral Surg. Oral Med. Oral Pathol. Oral Radiol.* **2019**, *127*, 247–256. [[CrossRef](#)] [[PubMed](#)]
37. Ibrahim, N.; Parsa, A.; Hassan, B.; van der Stelt, P.; Rahmat, R.A.; Ismail, S.M.; Aartman, I.H. Comparison of anterior and posterior trabecular bone microstructure of human mandible using cone-beam CT and micro CT. *BMC Oral Health* **2021**, *21*, 249. [[CrossRef](#)] [[PubMed](#)]
38. Tabassum, A.; Chainchel Singh, M.K.; Ibrahim, N.; Ramanarayanan, S.; Mohd Yusof, M.Y.P. Quantifications of Mandibular Trabecular Bone Microstructure Using Cone Beam Computed Tomography for Age Estimation: A Preliminary Study. *Biology* **2022**, *11*, 1521. [[CrossRef](#)] [[PubMed](#)]
39. Tayman, M.A.; Kamburoğlu, K.; Ocak, M.; Özen, D. Effect of different voxel sizes on the accuracy of CBCT measurements of trabecular bone microstructure: A comparative micro-CT study. *Imaging Sci. Dent.* **2022**, *52*, 171. [[CrossRef](#)] [[PubMed](#)]
40. El-Gizawy, A.S.; Ma, X.; Pfeiffer, F.; Schiffbauer, J.D.; Selly, T. Characterization of Microarchitectures, Stiffness and Strength of Human Trabecular Bone Using Micro-Computed Tomography (Micro-CT) Scans. *BioMed* **2023**, *3*, 89–100. [[CrossRef](#)]
41. Al-Khatib, A.; Rajion, Z.; Masudi, S.; Hassan, R.; Anderson, P.; Townsend, G. Tooth size and dental arch dimensions: A stereophotogrammetric study in Southeast Asian Malays. *Orthod. Craniofacial Res.* **2011**, *14*, 243–253. [[CrossRef](#)]
42. Lim, E.L.; Ngeow, W.C.; Lim, D. The implications of different lateral wall thicknesses on surgical access to the maxillary sinus. *Braz. Oral Res.* **2017**, *31*, e97. [[CrossRef](#)]
43. Hassani, A.; Khojasteh, A.; Shamsabad, A.N. The anterior palate as a donor site in maxillofacial bone grafting: A quantitative anatomic study. *J. Oral Maxillofac. Surg.* **2005**, *63*, 1196–1200. [[CrossRef](#)]
44. Carter, D.R.; Spengler, D.M. Mechanical properties and composition of cortical bone. *Clin. Orthop. Relat. Res. (1976–2007)* **1978**, *135*, 192–217. [[CrossRef](#)]
45. Parfitt, A.M.; Drezner, M.K.; Glorieux, F.H.; Kanis, J.A.; Malluche, H.; Meunier, P.J.; Ott, S.M.; Recker, R.R. Bone histomorphometry: Standardization of nomenclature, symbols, and units: Report of the ASBMR Histomorphometry Nomenclature Committee. *J. Bone Miner. Res.* **1987**, *2*, 595–610. [[CrossRef](#)] [[PubMed](#)]
46. Cömert, A.; Kökat, A.M.; Akkocaoğlu, M.; Tekdemir, İ.; Akça, K.; Çehreli, M.C. Fresh-frozen vs. embalmed bone: Is it possible to use formalin-fixed human bone for biomechanical experiments on implants? *Clin. Oral Implant. Res.* **2009**, *20*, 521–525. [[CrossRef](#)]
47. Holm, M.A.; Iazzo, P.A. Importance of Human Cadaver Studies in Education and Medical Device Research: Insights Derived from Various Imaging Studies and Modalities. In *Engineering in Medicine*; Elsevier: Amsterdam, The Netherlands, 2019; pp. 255–280.
48. Viidik, A.; Lewin, T. Changes in tensile strength characteristics and histology of rabbit ligaments induced by different modes of postmortal storage. *Acta Orthop. Scand.* **1966**, *37*, 141–155. [[CrossRef](#)]
49. Kivovics, M.; Szabó, B.T.; Németh, O.; Tari, N.; Dóri, F.; Nagy, P.; Dobó-Nagy, C.; Szabó, G. Microarchitectural study of the augmented bone following ridge preservation with a porcine xenograft and a collagen membrane: Preliminary report of a prospective clinical, histological, and micro-computed tomography analysis. *Int. J. Oral Maxillofac. Surg.* **2017**, *46*, 250–260. [[CrossRef](#)] [[PubMed](#)]
50. Trimmel, B.; Gyulai-Gaál, S.; Kivovics, M.; Jákob, N.P.; Hegedűs, C.; Szabó, B.T.; Dobó-Nagy, C.; Szabó, G. Evaluation of the histomorphometric and micromorphometric performance of a serum albumin-coated bone allograft combined with A-PRF for early and conventional healing protocols after maxillary sinus augmentation: A randomized clinical trial. *Materials* **2021**, *14*, 1810. [[CrossRef](#)] [[PubMed](#)]
51. Vasconcellos, L.M.R.D.; Leite, D.O.; Oliveira, F.N.D.; Carvalho, Y.R.; Cairo, C.A.A. Evaluation of bone ingrowth into porous titanium implant: Histomorphometric analysis in rabbits. *Braz. Oral Res.* **2010**, *24*, 399–405. [[CrossRef](#)] [[PubMed](#)]

52. Hildebrand, T.; Rüegsegger, P. Quantification of bone microarchitecture with the structure model index. *Comput. Methods Biomech. Bio Med. Eng.* **1997**, *1*, 15–23. [[CrossRef](#)]
53. Singh, I. The architecture of cancellous bone. *J. Anat.* **1978**, *127*, 305. [[PubMed](#)]
54. Goodchild, S.; Black, D.S.; Cunningham, C. A Qualitative and Quantitative Analysis of the Developing Human Lumbar Vertebral Column. Ph.D. Thesis, University of Dundee, Dundee, UK, 2019.
55. Ngeow, W.C.; Lim, D.; Tan, C.C.; Shetty, N.; Marla, V. 14-Dental Implant modifications for medically compromised patients. In *Dental Implants: Materials, Coatings, Surface Modifications and Interfaces with Oral Tissues*; Series in Biomaterials; Woodhead Publishing: Cambridge, UK, 2020; pp. 255–286.
56. Fanuscu, M.I.; Chang, T.L. Three-dimensional morphometric analysis of human cadaver bone: Microstructural data from maxilla and mandible. *Clin. Oral Implant. Res.* **2004**, *15*, 213–218. [[CrossRef](#)] [[PubMed](#)]

**Disclaimer/Publisher’s Note:** The statements, opinions and data contained in all publications are solely those of the individual author(s) and contributor(s) and not of MDPI and/or the editor(s). MDPI and/or the editor(s) disclaim responsibility for any injury to people or property resulting from any ideas, methods, instructions or products referred to in the content.